Effect of Residual Carbon on Spin-Polarized Coupling at a Graphene/Ferromagnet Interface

Matteo Jugovac,* Iulia Cojocariu, Francesca Genuzio, Chiara Bigi, Debashis Mondal, Ivana Vobornik, Jun Fujii, Paolo Moras, Vitaliy Feyer, Andrea Locatelli, and Tevfik Onur Menteş*

Vertical stacks of graphene and ferromagnetic layers are predicted to be efficient spin filters, while the experimentally observed figures of merit systematically remain below the theoretical predictions. According to general consensus, a vaguely defined interface contamination is found responsible for this discrepancy. Here, it is demonstrated how the spin-polarized electronic structure of single-layer graphene supported on a ferromagnetic cobalt substrate is affected by the presence of an interfacial carbidic buffer layer, formed by residual carbon present in the Co substrate. It is found that the Co-C hybridized single-spin state near the Fermi level disappears upon thermal segregation of bulk carbon at the graphene–Co interface, which determines the electronic decoupling of graphene from the ferromagnetic support and consequently, the suppression of net spin polarization. These observations are shown to be independent of the graphene azimuthal orientation with respect to the high symmetry directions of the substrate. The findings provide clear evidence that the realization of highly polarized spin currents in graphene/ferromagnet heterostacks depends on careful control of the graphene growth process in order to eliminate interfacial carbon.

1. Introduction

Discoveries of giant magnetoresistance and spin-transfer torque effect had a fundamental impact in the field of information storage, enabling control of the electron spin in a variety of devices that can read and write data with minimal thermal dissipation and energy loss.[1] An exemplary application is provided by spin valves, which are composed of two ferromagnetic layers separated by a non-magnetic spacer acting as a tunnel barrier.

Similar heterostructures comprising two-dimensional (2D) materials are under investigation, targeting reduced device sizes and improved efficiencies.[2] To this end, graphene stands out as one of the most promising candidates for usage in spintronics, as both high charge carrier mobility and small intrinsic spin–orbit coupling (SOC) favor long spin lifetime.[3] Moreover, graphene band-structure is significantly modified in proximity to a ferromagnet, allowing to control exchange interactions and achieving substantial SOC, which could be fruitfully exploited to realize logical devices.

In this context, cobalt-coupled graphene has attracted significant attention due to its unique electronic and magnetic properties.[4,5] The close proximity of graphene with cobalt produces a significant impact on graphene's electronic structure, leading to the shift of the Dirac cone away from the Fermi level. Moreover, a well-defined single-spin polarized band appears due to Co–C orbital hybridization. This band, typically referred to as "minicone,"[6] is characterized by a parabolic dispersion and an apex close to the Fermi level. Recently, we demonstrated that the band dispersion and spin-polarization of the "minicone" states do not depend on the azimuthal orientation of graphene with respect to the substrate's high symmetry directions.[7] This band arises exclusively due to the close interaction of graphene (Gr) with Co and is suppressed when foreign species are introduced at the graphene–Co interface.[8]

M. Jugovac, I. Cojocariu,[+] F. Genuzio, A. Locatelli, T. O. Menteş
Elettra – Sincrotrone Trieste S.C.p.A.
S.S. 14 km 163.5, 34149 Trieste, Italy
E-mail: matteo.jugovac@elettra.eu; tevfik.mentes@elettra.eu

The ORCID identification number(s) for the author(s) of this article can be found under https://doi.org/10.1002/aelm.202300031.

[+]Present address: Università degli studi di Trieste, Dipartimento di Fisica, Via A. Valerio 2, Trieste 34127, Italy

M. Jugovac, I. Cojocariu, V. Feyer
Peter Grünberg Institute (PGI-6)
Forschungszentrum Jülich GmbH
52425 Jülich, Germany

M. Jugovac, P. Moras
Istituto di Struttura della Materia-CNR (ISM-CNR)
34149 Trieste, Italy

C. Bigi, D. Mondal, I. Vobornik, J. Fujii
Istituto Officina dei Materiali IOM-CNR
Laboratorio TASC
34149 Trieste, Italy

D. Mondal
International Centre for Theoretical Physics (ICTP)
Strada Costiera 11, 34100 Trieste, Italy

Based on the spin-polarized band structure of graphene in contact with Ni and Co, vertical stacks of Ni/Gr/Ni and Co/Gr/Co were predicted to be very efficient spin filters.[9,10] On the experimental side, Chemical Vapor Deposition (CVD) growth of graphene gives better performance as a spin filter compared to wet transfer methods, which suffer from excessive contamination and oxidation of metallic constituents. Nevertheless, even devices based on CVD-grown graphene fail to attain the theoretically predicted efficiencies.[11]

Reasons for the underperformance of graphene-based spintronic devices can be sought in the interface chemistry. In relation to the sensibility of the graphene–ferromagnet interface to foreign species, a variety of intercalants such as lithium, silicon or oxygen were shown to result in an electronic decoupling specifically for graphene on Co, leading to the lifting of graphene spin polarization.[8,12,13] On the other hand, carbon is the most relevant constituent of any contamination that may result from the graphene growth or transfer processes. However, it is understandably also the most difficult element to characterize and control in a graphene-based system abundant in carbon. Thus, in the present work, by using a comprehensive spectromicroscopy approach, we study spin-polarized graphene band structure in the presence of excessive carbon, in the form of a metal carbide, at the graphene–Co interface. Such an interface is obtained by growing graphene on top of a carbon-enriched cobalt film. After CVD graphene growth, the sample is kept at a temperature favoring interface segregation of carbon, which readily forms a metal-carbide structure. We demonstrate that the carbidic interface layer remarkably modifies the electronic properties, approaching those of a quasi-freestanding graphene. By measuring spin-resolved momentum maps, we show that the carbidic layer lifts the hybridization present in the pristine interface, resulting in spin-unpolarized graphene bands. This spin-decoupling does not depend on the relative orientation of graphene and substrate at the interface, leading to the same behavior of the electronic structure for both aligned and rotated graphene domains.

2. Results

Co heterostacks were prepared as detailed in the Methods Section. Graphene was grown by exposing the Co(0001) film to 5×10^{-7} mbar partial pressure of ethylene (C_2H_4) for 900 s at about 840 K. This protocol resulted in the formation of a complete graphene layer exhibiting multiple rotational domains.[7] Subsequently, rotationally incoherent graphene was transformed into epitaxial graphene by following a well-established procedure involving dissolution of graphene's rotational domains and C recondensation into a new graphene layer in registry with the underlying cobalt.[14] After completion of the graphene epilayer (in the following named Gr/Co), the sample was rapidly cooled down to room temperature to avoid carbon segregation at the graphene-Co interface.

X-ray photoemission spectroscopy (XPS) at the C 1s core level allowed the chemical state of the Gr/Co sample to be fully characterized (**Figure 1**a top). The C 1s line-shape is nicely reproduced by a fit with the two components, corresponding to graphene carbon atoms in top (284.9 eV) and hollow (285.2 eV) adsorption sites, [15] respectively, along with a small shoulder at
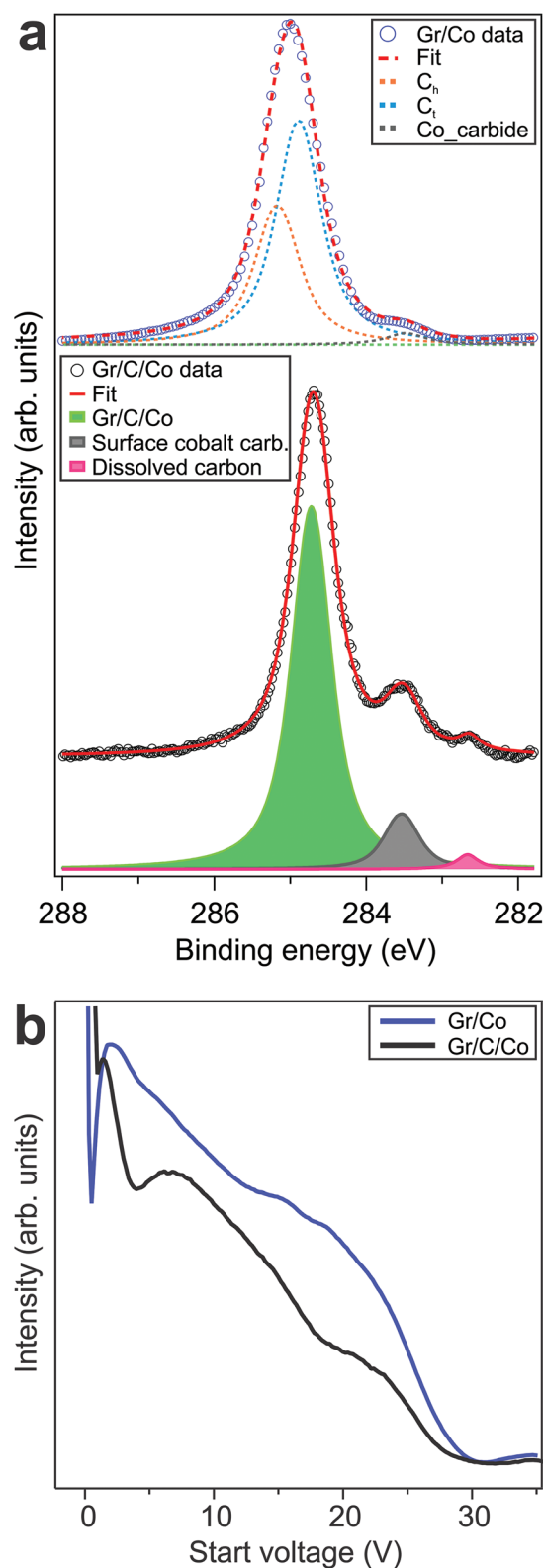
Figure 1. Spectroscopic characterization of Gr/Co and Gr/C/Co samples. a) XPS at the C 1s core level of the as-grown graphene on cobalt (top) and of the sample after carbon segregation leading to the formation of a cobalt carbide at the graphene-Co interface (bottom). b) LEEM-IV spectra of the two samples in (a).

lower binding energies (at about 283.5 eV). The low binding energy peak originates from the surface carbidic component, as reported in our previous studies.[14]

The carbide buffer layer between the graphene and cobalt was grown as follows. During the first step, the sample was annealed to 950 K, so that the previously obtained graphene epilayer could be dissolved. Subsequently, the bare Co surface was exposed to ethylene at a partial pressure of 5×10^{-7} mbar, at a temperature in the range from 520 to 570 K. Under such conditions, ethylene adsorbs dissociatively and C readily migrates below the surface, where it accumulates.[14] Finally, the specimen temperature was increased to 840 K and the CVD graphene growth was repeated at 5×10^{-7} mbar partial pressure of ethylene for 900 s. This preparation allowed the formation of rotated graphene, which was then partially realigned to obtain a film composed of both aligned and rotated domains.

Following this treatment, in order to favor surface segregation of bulk dissolved carbon, the graphene-covered Co film was annealed for 2 h at 570 K and finally cooled down to room temperature (in the following named Gr/C/Co). As seen in Figure 1a (bottom), the C 1s spectrum shows the main contribution peaked at around 284.5 eV. In addition, there are two distinct components at 283.5 eV and 282.8 eV binding energy, characteristic of surface carbides and bulk-dissolved atomic carbon, respectively.[14,16] The single-component main peak at binding energy close to that of bulk graphite can be assigned to a graphene layer on a carbon-rich phase, i.e., cobalt carbide. Indeed, the main C 1s peak area agrees well with that of the as-grown Gr/Co. Instead, the increase in intensity at low binding energies is consistent with surface/subsurface segregation of carbon. A quantitative comparison of intensities taking into account the electron attenuation length at the particular electron kinetic energy the carbide to graphene ratio is found to be 1:4, which is in agreement with a Co_2C structure at the interface underneath graphene. The low-energy electron diffraction (LEED) pattern (not shown) acquired after the formation of the carbidic layer did not present any additional spots as compared

to the as-synthesized graphene/cobalt interface, meaning that either the carbide adopts a (1×1) structure with respect to the cobalt substrate or that the carbide is not ordered.

We note that, the total amount of carbon one can dissolve in the Co film scales with its thickness. Therefore, the possibility to form interfacial carbide is favored in thick films, especially upon prolonged annealing. Importantly, our observations show that thermal treatments (for the formation of the graphene/carbide interface) do not alter the chemical state and morphology of the cobalt film. No signs of W 4f emission were in fact noted after the synthesis, as observed in our previous study.[14]

The different structure of Gr/Co and Gr/C/Co is confirmed by the low-energy electron reflectivity (LEEM-IV) curves displayed in Figure 1b. Whereas Gr/Co exhibits a featureless LEEM-IV curve, Gr/C/Co shows pronounced differences, especially in the region below 10 V, with a particularly pronounced dip at around 5 V. Notably, the differences between Gr/Co and Gr/C/Co LEEM-IV curves are reminiscent of those in the case of Gr/Ni(111) with and without a carbidic layer under graphene.[17]

The graphene-cobalt electronic structure was probed by means of angle-resolved photoemission spectroscopy (ARPES). In the case of the Gr/Co interface, owing to the strong Co–C interfacial interactions, the graphene π band shifts to higher binding energies by about 2.83 eV with respect to the freestanding case (**Figure 2**a). The "minicone" (orange arrow), originating from the C $2p_z$ and the Co 3d band (red arrow) hybridization, is clearly visible at the $\overline{K}$ point in the vicinity of the Fermi level.

Following carbon segregation at the interface and subsequent formation of the cobalt carbide layer, a significant change in the band structure is observed. The "minicone" band disappears, and the principal Dirac cone shifts to lower binding energies (Figure 2b). The shape and position of the graphene Dirac cone are analyzed using the intensity profile shown in Figure 2c taken across the $\overline{K}$ point along the direction perpendicular to the $\overline{\Gamma K}$ axis. Notably, the Co 3d band retains the same features as in the case of the as-grown Gr/Co film, apart from the sp-band (visible at around 1.1 $Å^{-1}$ in Figure 2b), which becomes more
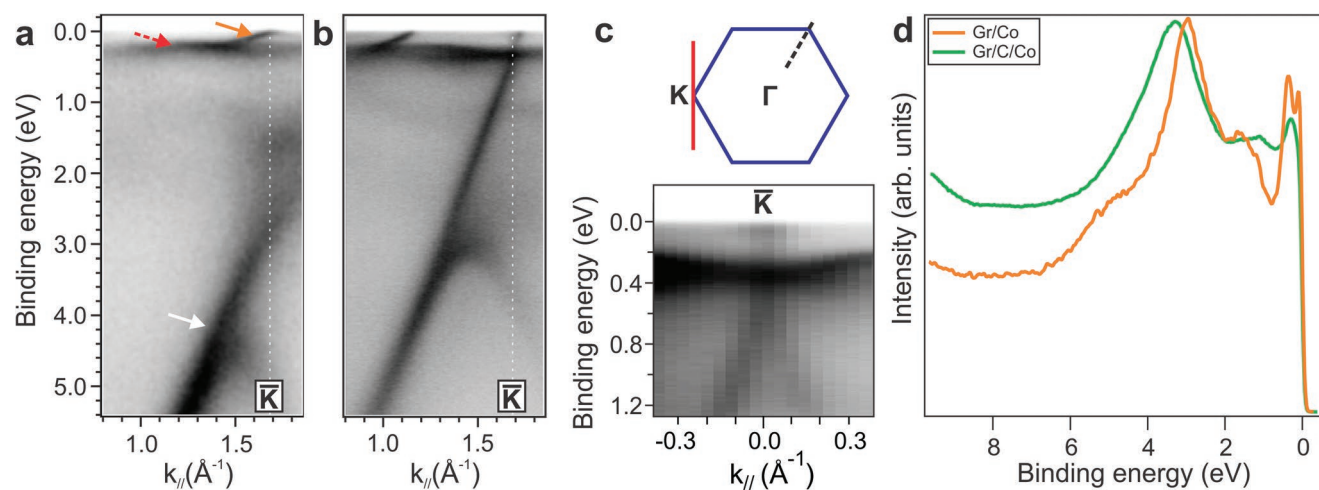
Figure 2. Electronic structure characterization of the two interfaces. Momentum maps of; a) Gr/Co, b) Gr/C/Co as a function of binding energy, acquired along the reciprocal space path indicated by the dashed line on the sketch of the BZ. The white arrow indicates the graphene π band, the "minicone" state is indicated by the orange arrow and the Co 3d band by the red arrow. c) Gr/C/Co momentum map along the solid red profile around the $\overline{K}$ point in the BZ sketch. d) Comparison of the EDCs (acquired at the $\overline{K}$ point) of the pristine Gr/Co and Gr/C/Co interfaces.

prominent. Instead, the Dirac cone undergoes a shift of about 2.6 eV compared to the as-grown Gr/Co system, resulting in a slight n-doping with the Dirac point found at around 0.23 eV below the Fermi level. The rotated domains behave in a similar fashion, with a slightly different binding energy of the Dirac point (0.29 eV).

The absence of the "minicone" band for the Gr/C/Co can also be observed in the energy-distribution curves (EDC) taken at the $\overline{K}$ point, as shown in Figure 2d. Consistently with the momentum maps in Figure 2b,c, the "minicone" intensity peak near the Fermi level is missing in the EDC of Gr/C/Co. Based on the spectroscopical and ARPES analysis, we, therefore, conclude that the interfacial layer is carbidic in nature and covers the entire graphene-Co interface uniformly. Moreover, no sign of a graphene bilayer is observed.

The presence of a single-spin nature of the "minicone" band in Gr/Co was confirmed by spin-resolved ARPES measurements, shown in **Figure 3**a. The features with higher intensity in the spin-integrated momentum map (Figure 3a, top) show a majority spin behavior (i.e., spin polarization > 0) as seen in the spin-resolved map (Figure 3a, bottom). Note that spin-polarization is also observed for other azimuthal graphene orientations, as reported in previous studies.[7] In addition, it is evident from Figure 3a that the sp-states of the Co substrate, visible around the center of the Brillouin zone (BZ), present strong minority spin polarization.

In the presence of a carbidic layer at the graphene-Co interface, i.e., in Gr/C/Co, the spin properties near the Fermi level are strongly altered, as seen in Figure 3b, which displays a combined spin-integrated (top) and spin-resolved (bottom) 2D momentum map acquired at a binding energy of 0.2 eV. Most importantly, the spin polarization at the $\overline{K}$ points of both aligned ($\overline{K}_{aligned}$) and rotated ($\overline{K}_{arc}$) graphene vanishes. This indicates that the graphene hybrid band loses its spin-polarization near the Fermi level (E_F) when it decouples from the Co substrate in the presence of the carbidic interface layer, independently from the azimuthal orientation of Gr/Co. Instead, Co bands in the proximity of $\overline{M}$ and $\overline{\Gamma}$ points, even if broader, preserve their majority and minority spin character, respectively.

On the other hand, spin-resolved EDCs of Gr/C/Co measured at the $\overline{K}$ point show a spin-asymmetry at higher binding energies between 0.2 and 0.4 eV binding energy. This energy region is identified with the Co 3d states visible both for Gr/Co and Gr/C/Co, as seen in Figure 2. No spin-asymmetry is detected outside this binding energy range. We note here (data not shown) that no out-of-plane spin polarization was observed at any binding energy in neither of the two samples.

3. Discussion

For ideal interfaces between graphene and ferromagnets (Ni and Co in particular), a high level of spin polarization of the 3d metal at the graphene $\overline{K}$ point was proposed to result in an efficient FM/Gr/FM spin filter.[9] In the same work, Karpan et al. discussed that the strong Gr–Co and Gr–Ni interactions would destroy the spin-polarized states near E_F, which was suggested to be remedied by adding Cu to the interface. In the following years, the electronic structure of graphene-Co and graphene-Ni
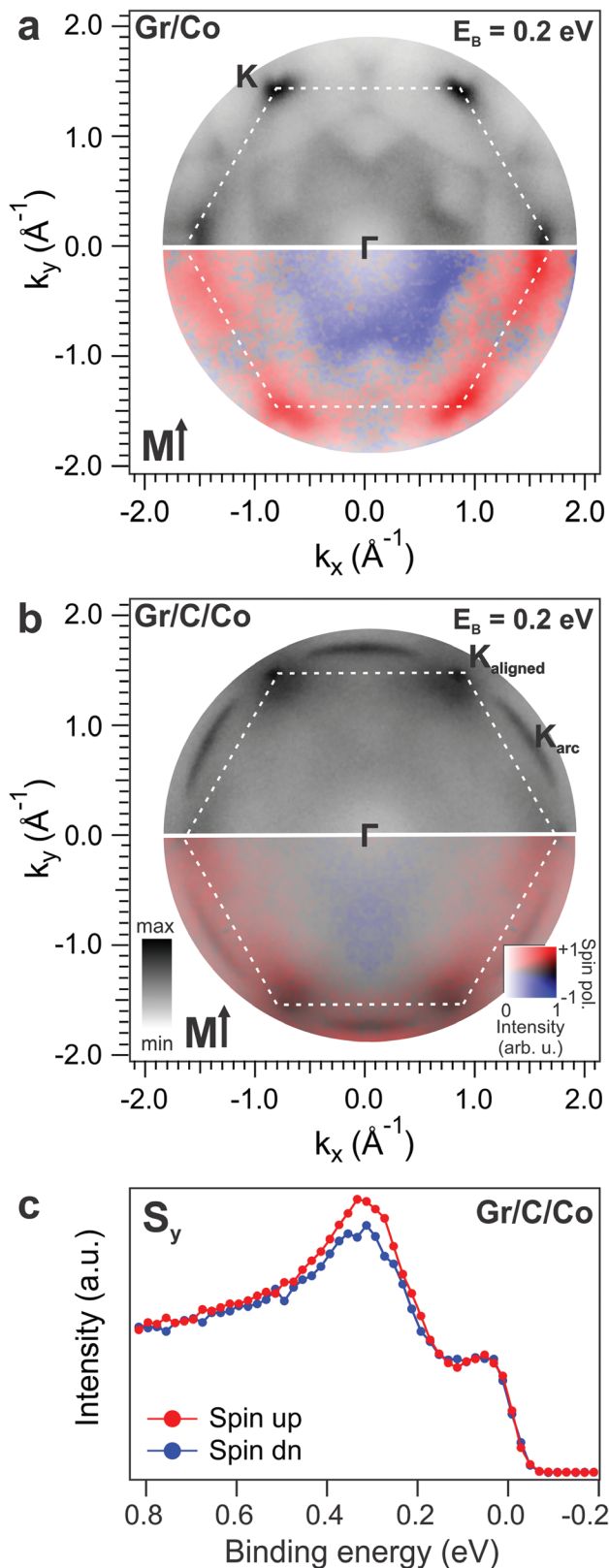
Figure 3. Combined spin-integrated (top) and spin-resolved (bottom) 2D momentum maps (acquired at 0.2 eV binding energy) of a) Gr/Co, b) Gr/C/Co. The intensity scales are indicated as insets. c) Spin-resolved EDC and polarization curves acquired at the $\overline{K}$ point of Gr/C/Co.

**ADVANCED
SCIENCE NEWS**

www.advancedsciencenews.com

**ADVANCED
ELECTRONIC
MATERIALS**
Open Access

www.advelectronicmat.de

interfaces were studied in more detail, revealing the spin-polarized "minicone" band near E_F,[6] which is present even for different azimuthal Gr–FM orientations.[7] These reports suggest that the strong Gr–FM interaction, in principle, does not extinguish the spin character at near E_F even in the presence of disorder due to the CVD process under realistic conditions.

Meanwhile, the experimentally attained efficiency of graphene spin-valves between two ferromagnets has not met the early expectations.[2] Mainly, the structural and chemical deviations from the ideal graphene–ferromagnet interface are likely responsible for the suppression of spin-related phenomena. Wet transfer methods have clear disadvantages, such as oxidation of the metal and residual contamination. CVD growth is reported to give better results in terms of device performance.[2,11]

On the other hand, an important aspect of the CVD process is the high carbon solubility in 3d transition metals at the relatively high temperatures involved. Indeed, carbon dissolution and segregation were shown to help recrystallize the graphene layer on Co with better structural quality.[14] Carbon present in the bulk is known to lead to the formation of a carbide layer between graphene and the Ni substrate via controlled thermal cycling.[17] The results here attest that a similar situation is also found for graphene on Co. The significance of carbidic carbon at the interface in terms of device physics is reflected in the data displayed in Figure 3, which demonstrates the disappearance of spin polarization at the graphene $\overline{K}$ point in the presence of interfacial carbide.

4. Conclusion

In conclusion, we demonstrate that in a system composed of a single layer of graphene lying on a carbon-rich cobalt film, carbon can be segregated, allowing the formation of a carbidic layer at the interface, as revealed by XPS and LEEM-IV. The presence of this buffer layer at the graphene-Co interface induces significant changes to the spin-polarized electronic properties. The spin-polarized "minicone" band disappears and the Dirac point shifts to 0.23 eV (0.29 eV) binding energy for aligned (rotated) graphene domains. While for the simple Gr/Co case, the orbital hybridization between graphene and cobalt determines the onset of a single-spin polarized ("minicone") band near the Fermi level, the presence of the interfacial carbide lifts the hybridization and suppresses the spin-polarization at the graphene $\overline{K}$ point at E_F. Importantly, the as-grown Gr/Co system can be, in principle, recovered by dissolving the interfacial carbon into the Co film, thus restoring the strong graphene-Co interaction. This leads to the following two consequences: residual carbidic carbon at the Gr–ferromagnet interface may have detrimental effects on the efficiency of a potential spin-based device; from the opposite perspective, controlled segregation/dissolution of interfacial carbide provides the means to modulate the spin-related properties, giving another degree of freedom in spintronic devices.

5. Experimental Section

Sample Preparation: W(110) single crystal substrate was cleaned by oxygen treatment (1×10^{-6} mbar of molecular oxygen; 1370 K) followed by high-temperature flashes to above 2250 K in UHV. A 10 nm cobalt film was deposited from a high-purity Co rod in an electron-beam evaporator. The resulting surface exhibited six sharp spots in LEED, characteristic of the unreconstructed Co(0001) surface crystalline structure. On Co films prepared in this way, graphene was grown by CVD method. The CVD growth was carried out at a temperature of 840 K in 5×10^{-7} mbar ethylene for 900 s. This preparation also allowed the formation of rotated graphene, which was partially realigned to obtain a sample composed of both aligned and rotated domains.

Experimental Methods: The experiments were performed at the Nanospectroscopy, NanoESCA, and APE-LE endstations of the Elettra Synchrotron in Trieste (Italy). The LEEM and LEED, as well as X-ray Photo-Emission Electron Microscopy (XPEEM) experiments, were carried out at the Nanospectroscopy beamline using the Spectroscopic Photoemission and Low Energy Electron Microscope (SPELEEM). This instrument combines the structural information from LEEM and LEED with the chemical/magnetic sensitivity of XPEEM.[18,19] The lateral resolution was around 10 nm in LEEM mode and 30 nm in XPEEM.[20,21]

Spin-resolved ARPES measurements were performed at the APE-LE beamline, using a photon energy of 40 eV, p-polarization, while keeping the sample at 80 K. The data were collected with a Scienta-Omicron-DA30 Scienta hemispherical analyzer that operates in deflection mode and provides a high-resolution k-space mapping of the Brillouin zone BZ while the sample geometry is kept fixed. The overall energy resolution was 80 meV, and the angular resolution was better than 0.2°. Spin-resolved spectra were acquired with VESPA VLEED-based spin spectrometer.[22]

The spin-resolved measurements covering the entire 2D Brillouin zone BZ were carried out at the NanoESCA beamline, using a photon energy of 40 eV, p-polarization. Instead, the XPS data for the pristine Gr/Co and the Gr/C/Co were acquired using a photon energy of 380 eV, s-polarization. All the measurements were performed while keeping the sample at 80 K. NanoESCA endstation hosts an electrostatic PEEM equipped with a double-pass hemispherical analyzer (Focus GmBH/Omicron NanoESCA II).[23] The instrument, in reciprocal space mode operation, was capable of detecting angle-resolved photoemission intensities simultaneously in the full-emission hemisphere above the sample surface. The photoemitted electrons were collected by an electron-optical column, energy-filtered in the double-hemispherical configuration (IDEA) and finally projected onto a 2D detector. By inserting a W(001) target within the imaging electron-optical column, energy-selective spin–orbit scattering of the photoemitted electrons allows for real or reciprocal space imaging with spin resolution.[24] In the 2D (spin-resolved) momentum maps at selected kinetic energy, the measured parallel momentum varies in the [−2; 2] Å^{-1} range. The binding energy scale was referenced to the Fermi level of the bare Co surface.

Acknowledgements

Conflict of Interest

The authors declare no conflict of interest.

Data Availability Statement

The data that support the findings of this study are available from the corresponding author upon reasonable request.

Keywords

[1] M. Shiraishi, M. Ohishi, R. Nouchi, N. Mitoma, T. Nozaki, T. Shinjo, Y. Suzuki, *Adv. Funct. Mater.* **2009**, *19*, 3711.

[2] M. Piquemal-Banci, R. Galceran, M.-B. Martin, F. Godel, A. Anane, F. Petroff, B. Dlubak, P. Seneor, *J. Phys. D* **2017**, *50*, 203002.

[3] Z. Han, A. Kimouche, D. Kalita, A. Allain, H. Arjmandi-Tash, A. Reserbat-Plantey, L. Marty, S. Pairis, V. Reita, N. Bendiab, J. Coraux, V. Bouchiat, *Adv. Funct. Mater.* **2014**, *24*, 3725.

[4] A. Varykhalov, D. Marchenko, J. Sánchez-Barriga, M. R. Scholz, B. Verberck, B. Trauzettel, T. O. Wehling, C. Carbone, O. Rader, *Phys. Rev. X* **2012**, *2*, 041017.

[5] F. Ajejas, A. Gudin, R. Guerrero, A. Anadón Barcelona, J. M. Diez, L. de Melo Costa, P. Olleros, M. A. Nino, S. Pizzini, J. Vogel, M. Valvidares, P. Gargiani, M. Cabero, M. Varela, J. Camarero, R. Miranda, P. Perna, *Nano Lett.* **2018**, *18*, 5364.

[6] D. Usachov, A. Fedorov, M. M. Otrokov, A. Chikina, O. Vilkov, A. Petukhov, A. G. Rybkin, Y. M. Koroteev, E. V. Chulkov, V. K. Adamchuk, A. Grüneis, C. Laubschat, D. V. Vyalikh, *Nano Lett.* **2015**, *15*, 2396.

[7] M. Jugovac, E. D. Donkor, P. Moras, I. Cojocariu, F. Genuzio, G. Zamborlini, G. Di Santo, L. Petaccia, N. Stojić, V. Feyer, C. M. Schneider, A. Locatelli, T. O. Menteş, *Carbon* **2022**, *163*, 198.

[8] M. Jugovac, F. Genuzio, T. O. Menteş, A. Locatelli, G. Zamborlini, V. Feyer, C. M. Schneider, *Carbon* **2020**, *163*, 341.

[9] V. M. Karpan, G. Giovannetti, P. A. Khomyakov, M. Talanana, A. A. Starikov, M. Zwierzycki, J. van den Brink, G. Brocks, P. J. Kelly, *Phys. Rev. Lett.* **2007**, *99*, 176602.

[10] V. M. Karpan, P. A. Khomyakov, A. A. Starikov, G. Giovannetti, M. Zwierzycki, M. Talanana, G. Brocks, J. van den Brink, P. J. Kelly, *Phys. Rev. B* **2008**, *78*, 195419.

[11] J.-F. Dayen, S. J. Ray, O. Karis, I. J. Vera-Marun, M. V. Kamalakar, *Appl. Phys. Rev.* **2020**, *7*, 011303.

[12] M. Jugovac, C. Tresca, I. Cojocariu, G. Di Santo, W. Zhao, L. Petaccia, P. Moras, G. Profeta, F. Bisti, *Phys. Rev. B* **2022**, *105*, L241107.

[13] D. Y. Usachov, A. V. Fedorov, O. Y. Vilkov, A. V. Erofeevskaya, A. S. Vopilov, V. K. Adamchuk, D. V. Vyalikh, *Phys. Solid State* **2015**, *57*, 1040.

[14] M. Jugovac, F. Genuzio, E. L. Gonzalez, N. Stojić, G. Zamborlini, V. Feyer, T. O. Mentes, A. Locatelli, C. M. Schneider, *Carbon* **2019**, *152*, 489.

[15] D. Y. Usachov, K. A. Bokai, D. E. Marchenko, A. V. Fedorov, V. O. Shevelev, O. Y. Vilkov, E. Y. Kataev, L. V. Yashina, E. Rühl, C. Laubschat, D. V. Vyalikh, *Nanoscale* **2018**, *10*, 12123.

[16] K. Kawashima, K. Shin, B. R. Wygant, J.-H. Kim, C. L. Cao, J. Lin, Y. J. Son, Y. Liu, G. Henkelman, C. B. Mullins, *ACS Appl. Energy Mater.* **2020**, *3*, 3909.

[17] C. Africh, C. Cepek, L. L. Patera, G. Zamborlini, P. Genoni, T. O. Menteş, A. Sala, A. Locatelli, G. Comelli, *Sci. Rep.* **2016**, *6*, 19734.

[18] A. Locatelli, E. Bauer, *J. Phys.: Condens. Matter* **2008**, *20*, 093002.

[19] E. Bauer, *Surface Microscopy with Low-Energy Electrons*, Springer-Verlag, New York, **2014**.

[20] A. Locatelli, L. Aballe, T. O. Menteş, M. Kiskinova, E. Bauer, *Surf. Interface Anal.* **2006**, *38*, 1554.

[21] T. O. Menteş, G. Zamborlini, A. Sala, A. Locatelli, *Beilstein J. Nanotechnol.* **2014**, *5*, 1873.

[22] C. Bigi, P. K. Das, D. Benedetti, F. Salvador, D. Krizmancic, R. Sergo, A. Martin, G. Panaccione, G. Rossi, J. Fujii, I. Vobornik, *J. Synchrotron Radiat.* **2017**, *24*, 750.

[23] C. Wiemann, M. Patt, I. P. Krug, N. B. Weber, M. Escher, M. Merkel, C. M. Schneider, *e-J. Surf. Sci. Nanotechnol.* **2011**, *9*, 395.

[24] C. Tusche, M. Ellguth, A. Krasyuk, A. Winkelmann, D. Kutnyakhov, P. Lushchyk, K. Medjanik, G. Schönhense, J. Kirschner, *Ultramicroscopy* **2013**, *130*, 70.